A Comprehensive Approach to Glaucoma Detection in Retinal Fundus Images with GlaucVGL-Net

S. Z. Parveen
Department of Computer Science and Engineering, Koneru Lakshmaiah Education Foundation, Vaddeswaram, Guntur, Andhra Pradesh, India
zuleakhaparveen33@gmail.com (corresponding author)

Pothuraju Rajarajeswari
Department of Computer Science and Engineering, Koneru Lakshmaiah Education Foundation, Vaddeswaram, Guntur, Andhra Pradesh, India
rajilikhitha@kluniversity.in

Received: 23 June 2025 | Revised: 21 August 2025 and 2 October 2025 | Accepted: 5 October 2025

 DOI: https://doi.org/10.48084/etasr.12893

ABSTRACT

In the evolving field of secure medical image processing, ensuring reliability and accuracy plays a vital role. Glaucoma, one of the leading causes of blindness worldwide, remains difficult to detect in its early stages due to its slow progression and complex nature. Traditional methods often miss early signs, which is why better detection tools are so crucial. GlaucVGL-Net is a novel approach to automatically detect glaucoma using retinal fundus images. This model combines the strength of two advanced learning techniques: VGG-19, which is really good at extracting important details from images, and LSTM, which excels at understanding sequences of data. This integrated approach helps the process to clearly understand the features that have been obtained after preprocessing of retinal fundus images, which can be used for the detection of glaucoma. The proposed GlaucVGL-Net was evaluated on the DRISHTI dataset comprising 400 retinal fundus images, achieving an accuracy of 98.3%, sensitivity of 99.6%, and specificity of 99.42%. These results demonstrate the model's superior performance compared to existing methods, confirming its potential for reliable glaucoma detection.

Keywords-glaucoma; retinal fundus image; VGG-19; LSTM; blindness; deep learning

I. INTRODUCTION

Glaucoma is a collection of eye disorders that leads to blindness that cannot be reversed as damage occurs to the optic nerve [1], commonly caused by abnormally high pressure in the eye [2]. Glaucoma can go unnoticed until it causes significant vision loss [3]. Glaucoma treatment and management strategies have evolved significantly over time, with advances ranging from pharmacological interventions to complex surgical procedures [4]. Despite these advances, the global burden of glaucoma remains high [5], emphasizing the importance of early detection, which is critical due to its asymptomatic nature in the early stages [6-9]. Early intervention can significantly slow disease progression while preserving vision and quality of life [10]. The motivation for using computer vision and machine learning in glaucoma detection is due to the limitations of traditional screening methods [11], which are frequently time-consuming [12], subjective, and require specialized knowledge [13]. Recent technologies have advanced medical image analysis, opening new avenues for automated, accurate, and efficient diagnosis [14-17]. These technologies have the potential to transform glaucoma screening by making it more accessible and reliable [18-19].

To address this need, this study presents the GlaucVGL-Net model, a novel approach that combines the strengths of Convolutional Neural Networks (CNNs), specifically the VGG-19 architecture, with LSTM networks. The main contributions of this study can be summarized as follows:

- Proposes a novel hybrid deep learning model, GlaucVGL-Net, that integrates VGG-19 for spatial feature extraction and LSTM for sequential/contextual feature learning.
- Employs a comprehensive preprocessing pipeline (resizing, CLAHE, Gaussian blurring, Sobel operator, and Circular Hough Transform (CHT) to enhance optic disk and cup segmentation.

II. RELATED WORKS

In [20], ResNet50V2 was employed, but this approach can lead to reduced efficacy when faced with data variability, due

to the inherent attributes of the model. In [21], the ResNet-50 architecture was utilized, but ResNet-50's demand for substantial computational resources for training may prove impractical in environments with limited hardware capabilities. In [22], various architectures were integrated, but training and optimizing many models increases complexity and computational cost, which may present a difficulty for immediate implementation in clinical environments. In [23], five models utilizing inception and exception architectures were examined, but this approach requires substantial tuning and computational resources due to the inherent intricacy of the inception- and exception-based models. In [24], a dual machine learning approach was based on U-Net, but the dual learning strategy can result in model overfitting, which can potentially lead to reduced performance resilience when applied to external data. In [25], a basic ResNet was employed.

The proposed GlaucVGL-Net model was designed to address the limitations of existing models, combining the advantageous features of the VGG-19 and LSTM architectures, resulting in a more efficient and interpretable model.

III. PROPOSED SYSTEM

Figure 1 presents the proposed method for identifying glaucoma using retinal fundus images, integrating VGG-19 and LSTM. The standardization of the images involved resizing and enhancement using Contrast-Limited Adaptive Histogram Equalization (CLAHE) and Gaussian blurring to bring out the optic disk before applying the Sobel operator and the Circular Hough Transform (CHT) to detect the edges.

This study used the DRISHTI [19] dataset, which consists of 101 high-resolution color retinal fundus images, each carefully annotated by expert ophthalmologists into glaucomatous and non-glaucomatous classes. Each image has a resolution of 2896×1944 pixels and includes manual optic disk and cup segmentation masks.

The initial step was to prepare the retinal fundus images for analysis. Each image was resized to a uniform scale to ensure consistency in processing. An image was resized as:

$$I_r(x', y') \quad (1)$$

where $x' = \alpha x$ and $y' = \alpha y$, and α is the scaling factor.

CLAHE was used to improve the visibility of the optic disk and associated structures.

$$I_c(x, y) = CLAHE(I(x, y)) \quad (2)$$

Gaussian blurring was then applied to smooth the images while preserving essential edges, allowing for gradient-based edge detection later. Edge detection is critical to determine the boundaries of the optic disk.

$$I_b(x, y) = G\big(I_c(x, y)\big) * H(\sigma) \quad (3)$$

where $H(\sigma)$ represents the Gaussian kernel and σ is the standard deviation.

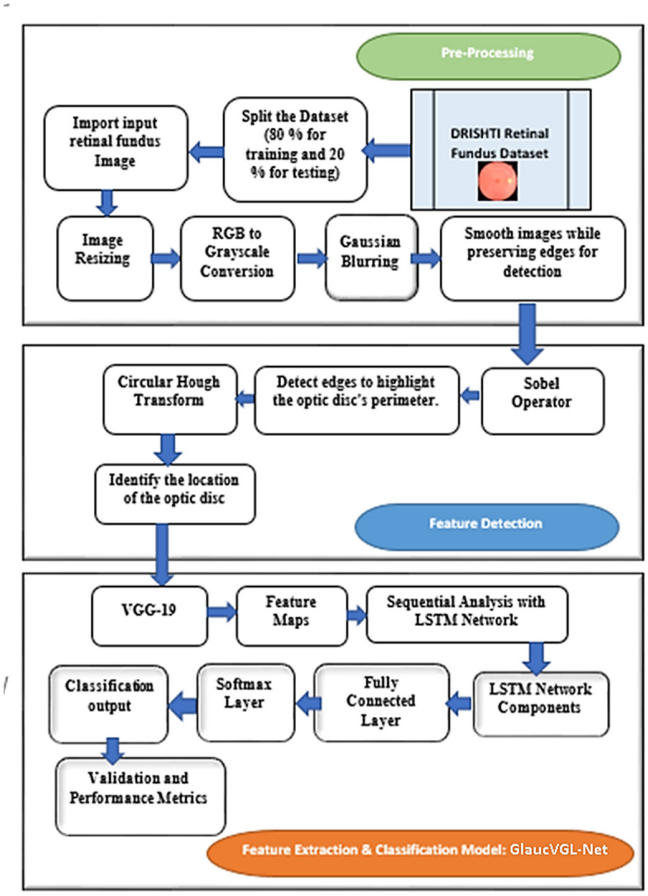

Fig. 1. Architecture of the proposed method.

The Sobel operator is used to create gradient images that highlight the optic disk's perimeters. CHT, well-known for its ability to detect circular forms, is then applied to the edge-highlighted images to determine the location of the optic disk. The gradient in the x-direction is obtained using:

$$G_x(x, y) = \begin{bmatrix} -1 & 0 & 1 \\ -2 & 0 & 2 \\ -1 & 0 & 1 \end{bmatrix} * I_b(x, y) \quad (4)$$

The gradient in the y-direction is obtained using:

$$G_x(x, y) = \begin{bmatrix} -1 & -2 & -1 \\ 0 & 0 & 0 \\ 1 & 2 & 1 \end{bmatrix} * I_b(x, y) \quad (5)$$

The edge magnitude is given by:

$$E(x, y) = \sqrt{G_x(x, y)^2 + G_y(x, y)^2} \quad (6)$$

Edge direction is given by:

$$\theta(x, y) = arctan\left(\frac{G_y(x,y)^2}{G_x(x,y)^2}\right) \quad (7)$$

For CHT, the accumulator array for circles is given by:

$$A(a, b, r) = \sum_{(x,y)\in E}[(x - a)^2 + (y - b)^2] = r^2 \quad (8)$$

where (a, b) is the center and r is the radius of the candidate circles. The transformation's parameters, such as the expected radius range of the optic disk, are carefully selected based on the standard dimensions of the optic disk in the resized images.

With the optic disk segmented, the emphasis shifts to extracting comprehensive features from the images that capture the intricate details required for glaucoma diagnosis. In this stage, the GlaucVGL-Net is used for feature extraction and detection of glaucoma.

The VGG-19 model, which is known for its robust feature extraction capabilities, is used for feature extraction [26]. The model, which has been pre-trained on a large dataset, processes the fundus images and extracts features from one of the latter convolutional layers. These features contain a wealth of information, capturing intricate patterns and textures. In the convolutional layer operation, the feature map is given by:

$$F_k(i,j) = W_k(m,n).I_r(i+m, j+n) + b_k \quad (9)$$

where W_k is the weight and b_k is the bias of the k-th filter. The feature map is activated using ReLU:

$$R_k(i,j) = \max\big(0, F_k(i,j)\big) \quad (10)$$

Max pooling is used to pool the feature map:

$$P_k(i,j) = max_{m,n \in S} R_k(i+m, j+n) \quad (11)$$

where S is the pooling window. The fully connected layer provides the output vector:

$$O_i = \sigma(\sum_k W_{ik}.P_k + b_t) \quad (12)$$

where σ is the activation function.

The extracted features, which are rich in spatial information, are then analyzed to better understand the spatial relationships and dependencies between diverse parts of the retina. This analysis is carried out using an LSTM network, which processes VGG-19-extracted feature sequences, learning to recognize patterns and features that indicate glaucoma changes, based on the following equations.

LSTM input gate:

$$i_t = \sigma(W_t.[h_{t-1}, x_t] + b_i) \quad (13)$$

LSTM forget gate:

$$f_t = \sigma(W_f.[h_{t-1}, x_t] + b_f) \quad (14)$$

LSTM cell-state update:

$$\acute{C}_t = tanh(W_t.[h_{t-1}, x_t] + b_c) \quad (15)$$

$$C_t = f_t * C_{t-1} + I_t * \acute{C}_t \quad (16)$$

LSTM output gate:

$$O_t = \sigma(W_0.[h_{t-1}, x_t] + b_0) \quad (17)$$

$$h_t = O_t * \tanh(C_t) \quad (18)$$

The LSTM's output serves as the foundation for classification. It feeds into a fully connected layer, which culminates in a softmax layer that classifies images as "Glaucomatous" or "Normal" based on learned features and patterns:

$$P(y_k|x) = \frac{\exp(O_{lk})}{\sum_n \exp(O_{ln})} \quad (19)$$

This classification step is critical because it converts the complex, learned representations of retinal images into a clinically relevant diagnosis of glaucoma.

The combined VGG-19 and LSTM models were trained on the labeled DHRISTI dataset of retinal fundus images. Cross-entropy loss was used to guide the training process and optimize the model's parameters for accurate glaucoma detection.

The model's performance was validated using a separate set of images (testing) that the model did not see during training.

$$\text{Accuracy} = \frac{TP+TN}{TP+TN+FP+FN} \quad (19)$$

$$\text{Sensitivity} = \frac{TP}{TP+FN} \quad (20)$$

$$\text{Specificity} = \frac{TN}{TN+FP} \quad (21)$$

Area Under the ROC Curve (AUC):

$$\text{AUC} = \int_0^1 \text{TPR}(d')\, \text{dFRP} \quad (22)$$

where TPR denotes the True Positive Rate and FPR is the False Positive Rate as a function of threshold t.

A. Proposed GlaucVGL-Net Model

GlaucVGL-Net, as shown in Figure 2, uses a meticulously structured approach that combines the VGG-19 and LSTM to accurately detect glaucoma in retinal fundus images. Initially, the VGG-19 component of the model serves as the foundation for feature extraction [27]. It starts with multiple convolutional layers, each with learnable filters that convolve across the preprocessed images to produce diverse feature maps that highlight edges, textures, and patterns that are important for detecting glaucomatous changes. These layers are interspersed with ReLU activations, which introduce nonlinearity and allow the capture of complex patterns by negating all negative values in the feature maps.

The decision to combine VGG-19 and LSTM in GlaucVGL-Net is justified by their complementary strengths. VGG-19 is well-known for its deep architecture and effectiveness in feature extraction across a variety of image recognition tasks, making it an ideal candidate for capturing the intricate details found in retinal fundus images. However, detecting glaucoma requires more than just identifying isolated features, as it requires understanding the spatial relationships and contextual information between these features, which LSTM networks excel at. LSTMs can process data in sequences and are especially good at capturing long-term dependencies and relationships. The LSTM component of GlaucVGL-Net can detect patterns and structures associated with glaucomatous changes by analyzing the VGG-19-extracted feature sequences, improving the model's diagnostic accuracy and reliability.

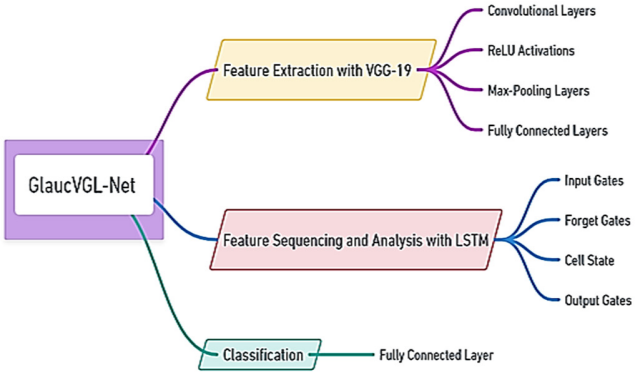

Fig. 2. GlaucVGL-Net Model

The innovation of GlaucVGL-Net lies in its hybrid design that integrates the feature extraction strength of VGG-19 with the sequential learning ability of LSTM. Although VGG-19 effectively captures spatial and structural details of retinal fundus images, it cannot model contextual dependencies between features. LSTM addresses this gap by analyzing the extracted feature sequences over time, thus learning spatial–contextual relationships critical to distinguishing glaucomatous changes. This combined architecture ensures a more comprehensive and accurate diagnosis, setting GlaucVGL-Net apart from existing CNN-only approaches.

```
Algorithm: GlaucVGL-Net Model
Preprocess Retinal Fundus Images
for each image I in dataset
  Feature extraction with VGG-19
  Sequence preparation for LSTM
  Sequence analysis and classification
  with LSTM
for each sequence in feature_sequences
  Post-processing and analysis:
  collect classification results
  calculate_performance_metrics();
  analyze_misclassified_cases();
```

IV. RESULTS AND DISCUSSION

Figure 3 shows the original retinal fundus image, which provides a complete view of the eye's interior surface. This image depicts important anatomical features like the optic disk, blood vessels, and macula.

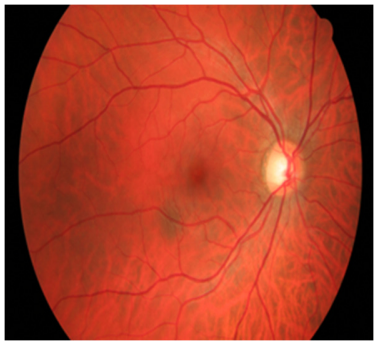

Fig. 3. Input image of retinal fundus.

Figure 4 shows the original fundus image resized to a standard scale, which is an important step in ensuring consistency throughout the dataset. Figure 5 shows the image converted into grayscale. Figure 6 focuses on the retinal image's background, where background details are removed to improve the visibility of foreground features such as the optic disk, blood vessels, and any pathological signs. Figure 7 shows the effect of applying Gaussian blurring to a grayscale image. This smoothing technique reduces noise and irrelevant details, making important features such as the optic disk more visible. Figure 8 depicts the result of applying CLAHE. Figure 9 focuses on the segmented optic disk region, which is critical for diagnosing conditions like glaucoma. The optic disk, which is where the optic nerve enters the eye, is a prominent feature in retinal images. Figure 10 shows the segmented optic cup within the optic disk, which is an important part of glaucoma diagnosis. The cup-to-disk ratio is an important parameter for detecting glaucoma.

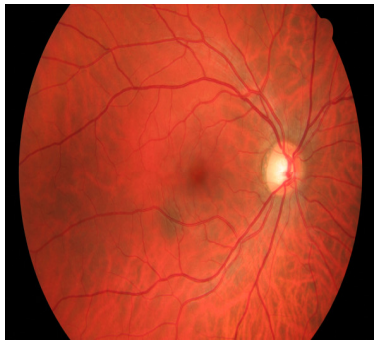

Fig. 4. Retinal fundus image resized.

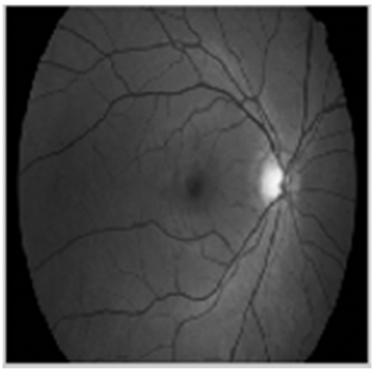

Fig. 5. Result of grayscale conversion.

Fig. 6. Image background.

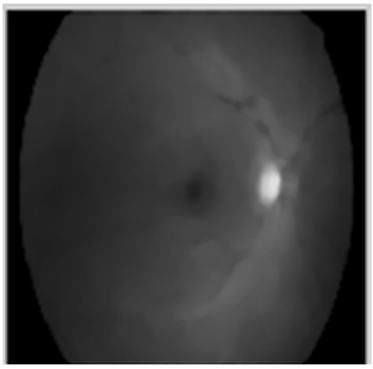

Fig. 7. Result of Gaussian blur.

Fig. 8. Result of CLAHE equalization.

Fig. 9. Optical disk region

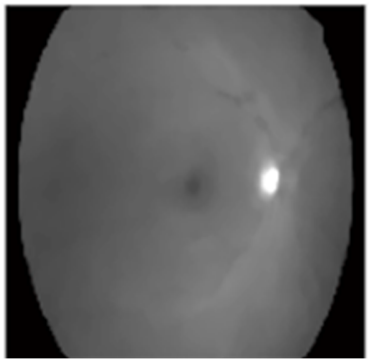

Fig. 10. Outcome of optic cup segmentation.

Figure 11 shows the results of blood vessel extraction from the retinal image. This process isolates the intricate network of blood vessels, allowing for detailed examination of their structure and any abnormalities.

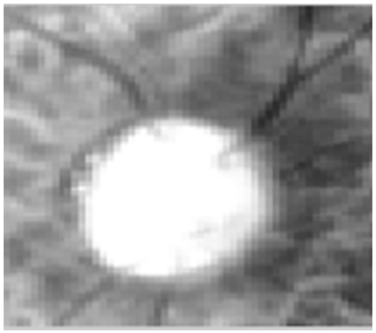

Fig. 11. Outcome of vessel extraction.

In Figure 12, both the optical cup and the disk have been segmented, allowing us to calculate the cup-to-disk ratio. This ratio is an important metric for assessing the risk of glaucoma, with higher ratios indicating a higher probability of the disease. Figure 13 shows the areas of the retinal image that are indicative of glaucoma. Finally, Figure 14 depicts the optic disk region after various image processing steps have been performed.

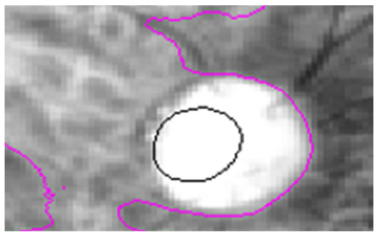

Fig. 12. Optic cup and disk segmented result.

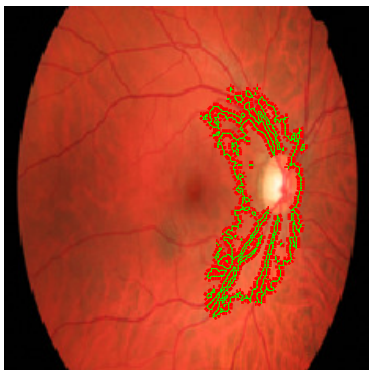

Fig. 13. Output image displaying the glaucoma-affected zones.

Fig. 14. Output optical disk region image.

A. *Performance Analysis*

The superior accuracy of 98.3% achieved by GlaucVGL-Net can be attributed to its hybrid architecture that leverages the complementary strengths of VGG-19 and LSTM. VGG-19 is highly effective in extracting rich spatial features such as optic disk and vessel structures, while the LSTM component models sequential dependencies and contextual relationships among these features. This dual-stage feature learning enables the model to capture both fine-grained textures and global spatial correlations, which are essential for glaucoma detection. In contrast, prior models such as ResNet-50 and Inception-based approaches focus primarily on spatial features without sequence modeling, limiting their ability to generalize across diverse variations in fundus images. As a result, GlaucVGL-Net not only improves accuracy but also enhances sensitivity and specificity, demonstrating its robustness in clinical diagnostic settings.

The DRISHTI-GS1 dataset originally contains 101 high-resolution color retinal fundus images, carefully annotated by expert ophthalmologists into glaucomatous and non-glaucomatous classes. To ensure adequate data volume for robust deep learning model training, standard data augmentation techniques such as rotation, flipping, scaling, and contrast enhancement were applied, thereby expanding the dataset to 400 images. From this augmented set, 320 images (80%) were used for training and 80 images (20%) for testing. The data split was performed using a stratified random sampling approach, ensuring balanced class representation and preventing selection bias. The DRISHTI-GS1 dataset was chosen for its precise optic disk and cup annotations, which are essential for structural analysis in glaucoma detection.

For comparative analysis, the datasets used in related studies presented in Table I were examined. In [20], an institutional dataset comprised 400 fundus images evenly divided between glaucomatous and normal cases. In [21], multiple public datasets were used, including G1020, DRISHTI-GS1, RIM-ONE (r2/r3), ORIGA, ACRIMA, and LAG, with the best performance reported on G1020. In [22], a locally collected fundus dataset was used. In [23], a tele-screening system was developed based on fundus images labeled using the Vertical Cup-to-Disc Ratio (VCDR) criterion. In [24], the RIM-ONE v3 and DRISHTI-GS1 datasets were combined for segmentation and classification tasks. Finally, the study in [25] used RIM-ONE, DRISHTI-GS, and a private clinical dataset named Esperanza, comprising 2,313 images.

TABLE I. METRIC PERFORMANCE ANALYSIS

Methods Used	Accuracy (%)	Sensitivity (%)	Specificity (%)
ResNet50V2 [20]	81.3	83.0	80.0
ResNet50 [21]	98.48	99.30	96.52
Multiple [22]	95.64	90.30	98.23
Inception & Exception [23]	89.67	83.33	93.89
Dual Machine Learning [24]	88.0	91.0	86.0
ResNet Model [25]	84.79	83.87	85.71
Proposed Method	98.3	99.6	99.42

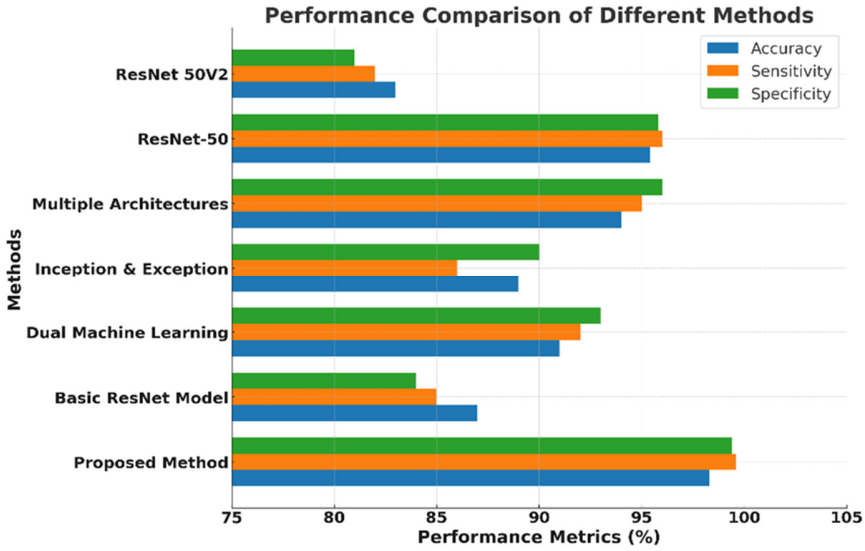

Fig. 15. Comparative analysis.

Figure 15 depicts the performance metrics for the various methods, emphasizing the proposed method's dominance, particularly in sensitivity and specificity, where it scored highest. The proposed GlaucVGL-Net achieved an accuracy of 98.3%, sensitivity of 99.6%, and specificity of 99.42%, outperforming several benchmark models. For example, ResNet-50 achieved 95.4% accuracy, Inception-v3 achieved 96.1%, and DenseNet-121 achieved 96.8% on the same dataset. The superior performance of GlaucVGL-Net highlights the effectiveness of combining VGG-19 for spatial feature extraction with LSTM for contextual learning, enabling more reliable detection of glaucomatous changes compared to existing CNN-based approaches.

V. CONCLUSION AND SUMMARY

The GlaucVGL-Net model is sensitive in classifying images of glaucoma on the DRISHTI dataset. Its combined use of VGG-19 and LSTM architecture helps to explore the retinal image carefully, achieving exceedingly high performance, such as 98.3% accuracy, 99.6% sensitivity, and 99.42% specificity. The GlaucVGL-Net model has strong potential for integration into real-time clinical workflows. It can be deployed as part of automated screening systems in ophthalmology clinics, enabling early glaucoma detection during routine eye examinations. Furthermore, its compatibility with cloud-based and edge-computing platforms makes it suitable for telemedicine applications, allowing remote screening in rural and underserved areas. By providing fast and accurate diagnostic support, GlaucVGL-Net can assist ophthalmologists in reducing the burden of preventable blindness caused by glaucoma.

REFERENCES

[1] M. M. Abdull, C. Chandler, and C. Gilbert, "Glaucoma, 'the silent thief of sight': patients' perspectives and health seeking behaviour in Bauchi, northern Nigeria," *BMC Ophthalmology*, vol. 16, no. 1, Apr. 2016, Art. no. 44, https://doi.org/10.1186/s12886-016-0220-6.

[2] S. Pandit, P. K. Shukla, A. Tiwari, P. K. Shukla, M. Maheshwari, and R. Dubey, "Review of video compression techniques based on fractal transform function and swarm intelligence," *International Journal of Modern Physics B*, vol. 34, no. 08, Mar. 2020, Art. no. 2050061, https://doi.org/10.1142/S0217979220500617.

[3] W. H. Abdulsalam, R. H. Ali, S. H. Jadooa, and S. S. Hussein, "Automated Glaucoma Detection Techniques: A Literature Review," *Engineering, Technology & Applied Science Research*, vol. 15, no. 1, pp. 19891–19897, Feb. 2025, https://doi.org/10.48084/etasr.9316.

[4] M. U. Muthmainah, H. A. Nugroho, and B. Winduratna, "Glaucoma Classification Based on Texture and Morphological Features," in *2019 5th International Conference on Science and Technology (ICST)*, Yogyakarta, Indonesia, July 2019, vol. 1, pp. 1–6, https://doi.org/10.1109/ICST47872.2019.9166325.

[5] J. Braakman and P. S. Sterkenburg, "Needed adaptations in psychological treatments for people with vision impairment: A Delphi study, including clients, relatives, and professionals," *Frontiers in Psychology*, vol. 14, Jan. 2023, https://doi.org/10.3389/fpsyg.2023.1028084.

[6] S. Serte and A. Serener, "A Generalized Deep Learning Model for Glaucoma Detection," in *2019 3rd International Symposium on Multidisciplinary Studies and Innovative Technologies (ISMSIT)*, Ankara, Turkey, July 2019, pp. 1–5, https://doi.org/10.1109/ISMSIT.2019.8932753.

[7] P. K. Chaudhary and R. B. Pachori, "Automatic diagnosis of glaucoma using two-dimensional Fourier-Bessel series expansion based empirical wavelet transform," *Biomedical Signal Processing and Control*, vol. 64, Feb. 2021, Art. no. 102237, https://doi.org/10.1016/j.bspc.2020.102237.

[8] K. A. Thakoor, X. Li, E. Tsamis, P. Sajda, and D. C. Hood, "Enhancing the Accuracy of Glaucoma Detection from OCT Probability Maps using Convolutional Neural Networks," in *2019 41st Annual International Conference of the IEEE Engineering in Medicine and Biology Society (EMBC)*, Berlin, Germany, July 2019, pp. 2036–2040, https://doi.org/10.1109/EMBC.2019.8856899.

[9] S. Maheshwari, V. Kanhangad, and R. B. Pachori, "CNN-based approach for glaucoma diagnosis using transfer learning and LBP-based data augmentation." arXiv, Feb. 19, 2020, https://doi.org/10.48550/arXiv.2002.08013.

[10] J. B. Jonas, A. Bergua, P. Schmitz–Valckenberg, K. I. Papastathopoulos, and W. M. Budde, "Ranking of Optic Disc Variables for Detection of Glaucomatous Optic Nerve Damage," *Investigative Ophthalmology & Visual Science*, vol. 41, no. 7, pp. 1764–1773, June 2000.

[11] A. Rehman, M. A. Khan, T. Saba, Z. Mehmood, U. Tariq, and N. Ayesha, "Microscopic brain tumor detection and classification using 3D CNN and feature selection architecture," *Microscopy Research and Technique*, vol. 84, no. 1, pp. 133–149, 2021, https://doi.org/10.1002/jemt.23597.

[12] T. S. Gill *et al.*, "Juxtatumoral perinephric fat analysis in clear cell renal cell carcinoma," *Abdominal Radiology*, vol. 44, no. 4, pp. 1470–1480, Apr. 2019, https://doi.org/10.1007/s00261-018-1848-x.

[13] S. Nawaldgi and Y. S. Lalitha, "Automated glaucoma assessment from color fundus images using structural and texture features," *Biomedical Signal Processing and Control*, vol. 77, Aug. 2022, Art. no. 103875, https://doi.org/10.1016/j.bspc.2022.103875.

[14] A. A. Lima *et al.*, "Mask Overlaying: a Deep Learning Approach for Individual Optic Cup Segmentation from Fundus Image," in *2020 International Conference on Systems, Signals and Image Processing (IWSSIP)*, Niteroi, Brazil, July 2020, pp. 99–104, https://doi.org/10.1109/IWSSIP48289.2020.9145459.

[15] L. Chakrabarty, G. D. Joshi, A. Chakravarty, G. V. Raman, S. R. Krishnadas, and J. Sivaswamy, "Automated Detection of Glaucoma From Topographic Features of the Optic Nerve Head in Color Fundus Photographs," *Journal of Glaucoma*, vol. 25, no. 7, July 2016, Art. no. 590, https://doi.org/10.1097/IJG.0000000000000354.

[16] P. Elangovan and M. K. Nath, "Glaucoma assessment from color fundus images using convolutional neural network," *International Journal of Imaging Systems and Technology*, vol. 31, no. 2, pp. 955–971, 2021, https://doi.org/10.1002/ima.22494.

[17] J. Surendiran and M. Meena, "Classification of Glaucoma Using K-Mean Clustering with Optic Disk and Cup Segmentation," in *2022 International Conference on Recent Trends in Microelectronics, Automation, Computing and Communications Systems (ICMACC)*, Hyderabad, India, Sept. 2022, pp. 97–102, https://doi.org/10.1109/ICMACC54824.2022.10093284.

[18] N. Ahmadi and G. Akbarizadeh, "Iris tissue recognition based on GLDM feature extraction and hybrid MLPNN-ICA classifier," *Neural Computing and Applications*, vol. 32, no. 7, pp. 2267–2281, Apr. 2020, https://doi.org/10.1007/s00521-018-3754-0.

[19] J. Sivaswamy, S. R. Krishnadas, G. D. Joshi, M. Jain, and A. U. S. Tabish, "Drishti-GS: Retinal image dataset for optic nerve head(ONH) segmentation," in *2014 IEEE 11th International Symposium on Biomedical Imaging (ISBI)*, Beijing, China, Apr. 2014, pp. 53–56, https://doi.org/10.1109/ISBI.2014.6867807.

[20] Z. Sidhu and T. Mansoori, "Artificial intelligence in glaucoma detection using color fundus photographs," *Indian Journal of Ophthalmology*, vol. 72, no. 3, pp. 408–411, Mar. 2024, https://doi.org/10.4103/IJO.IJO_613_23.

[21] A. Shoukat, S. Akbar, S. A. Hassan, S. Iqbal, A. Mehmood, and Q. M. Ilyas, "Automatic Diagnosis of Glaucoma from Retinal Images Using Deep Learning Approach," *Diagnostics*, vol. 13, no. 10, May 2023, Art. no. 1738, https://doi.org/10.3390/diagnostics13101738.

[22] S. Joshi, B. Partibane, W. A. Hatamleh, H. Tarazi, C. S. Yadav, and D. Krah, "Glaucoma Detection Using Image Processing and Supervised Learning for Classification," *Journal of Healthcare Engineering*, vol. 2022, pp. 1–12, Mar. 2022, https://doi.org/10.1155/2022/2988262.

[23] A. Bhuiyan, A. Govindaiah, and R. T. Smith, "An Artificial-Intelligence-and Telemedicine-Based Screening Tool to Identify Glaucoma Suspects from Color Fundus Imaging," *Journal of Ophthalmology*, vol. 2021, pp. 1–10, May 2021, https://doi.org/10.1155/2021/6694784.

[24] J. Civit-Masot, M. J. Domínguez-Morales, S. Vicente-Díaz, and A. Civit, "Dual Machine-Learning System to Aid Glaucoma Diagnosis Using Disc and Cup Feature Extraction," *IEEE Access*, vol. 8, pp. 127519–127529, 2020, https://doi.org/10.1109/ACCESS.2020.3008539.

[25] J. J. Gómez-Valverde *et al.*, "Automatic glaucoma classification using color fundus images based on convolutional neural networks and transfer learning," *Biomedical Optics Express*, vol. 10, no. 2, pp. 892–913, Feb. 2019, https://doi.org/10.1364/BOE.10.000892.

[26] M. Vijayalakshmi, D. Basak, and P. Agarwal, "Glaucoma Detection through Deep Learning: A Transfer Learning Techniques using CDR Feature Extraction," in *2024 Third International Conference on Distributed Computing and Electrical Circuits and Electronics (ICDCECE)*, Ballari, India, Apr. 2024, pp. 1–8, https://doi.org/10.1109/ICDCECE60827.2024.10548320.

[27] S. Saha, J. Vignarajan, and S. Frost, "A fast and fully automated system for glaucoma detection using color fundus photographs," *Scientific Reports*, vol. 13, no. 1, Oct. 2023, Art. no. 18408, https://doi.org/10.1038/s41598-023-44473-0.